

One-Step Synthesis of ZnO Films by Chemical Bath Deposition Not Using Thermal Annealing

T. Mendivil-Reynoso^{a*} , M. Flores-Acosta^b, M. Cortez-Valadez^c, R. Ochoa-Landin^a, S.J Castillo^b,
L.P. Ramírez-Rodríguez^a

^aUniversidad de Sonora, Departamento de Física, Calle Rosales y Blvd. Luis Encinas Johnson S/N, 83000, Hermosillo, México.

^bUniversidad de Sonora, Departamento de Investigación en Física, Apdo. Postal 588, 83190, Hermosillo, México.

^cUniversidad de Sonora, CONAHCYT-Departamento de Investigación en Física, Apdo. Postal 5-88, 83190, Hermosillo, México.

Received: September 20, 2023; Revised: November 21, 2023; Accepted: January 16, 2024

The novelty of the present study lies in synthesized ZnO film in a single step by chemical bath deposition. The typical conversion of zinc hydroxide ($\text{Zn}(\text{OH})_2$) into ZnO material through thermal annealing is not required. A direct synthesis has achieved using four different zinc salt sources, yielding equivalent results. All the synthesized ZnO films were non-specular and adhered well to the glass slide substrates. We present the results of the structural, optical, and morphological characterization techniques. These revealed a hexagonal structure, a band-gap energy of around 3.2 eV, and a hexagonal nanorod shape for all the synthesized ZnO films.

Keywords: ZnO, Synthesis by CBD, Optical and morphologic properties.

1. Introduction

The attribute extensive use of silicon as a semiconductor it is because of its properties and abundance. It is compatible with manufacturing processes: lithography, etching, doping, oxidation, deposition, and bonding. In recent years, development alternative semiconductor materials have been attention from research groups. Which allows for fulfilling the features or needs that silicon lacks and is compatible with manufacturing processes. Zinc selenide (ZnSe), gallium arsenide (GaAs), cadmium sulfide (CdS), and zinc oxide (ZnO) are some of the most studied and reported as alternative semiconductors. Researchers have studied ZnO for its photocatalytic, piezoelectric, and biocompatibility properties¹⁻⁴. It is a semiconductor material with a direct band gap of about 3.3 eV^{1,2,5,6}. It has a reported wurtzite-like structure⁷, with an exciton binding energy of 60 meV⁸, and a whole effective mass of 59 meV⁸. Because of this, there are studies of ZnO for application in medicine, electronics, among other fields⁹⁻¹³. Its high conductivity and optical transmittance identify it as promising for active layers in thin film transistors¹⁴. The piezoelectric properties of ZnO have made it an object of study for micro-electromechanical systems research (MEMS)¹⁵. Another example is the study of Schottky diodes fabricated from ZnO for use as highly effective ultraviolet photodetectors¹⁶. There is the use of nanostructured films based on ZnO as n-type semiconductor in solar cells to increase the effective absorption area¹⁷.

The broad areas of ZnO application have made it important to find simple ways to synthesize ZnO as a film. Therefore, there are different techniques employed for ZnO film synthesis. These methods are spray pyrolysis^{18,19}, chemical bath deposition (CBD)²⁰, chemical vapor deposition²¹, sputtering²², among others.

Because of its simplicity and low-cost, chemical solution deposition is a helpful technique for the synthesis of ZnO films. However, the metal oxides deposited using this technique contain a main phase of hydroxide of the metal or a proportion of it^{23,24}.

For this reason, the synthesis of ZnO films implies annealing process to the as-deposited films to achieve material. This is for as-deposited films, usually made up of zinc hydroxide ($\text{Zn}(\text{OH})_2$), into the oxide phase^{23,25}.

Using the method that we present in this work, a direct deposition of ZnO films in just one step without an annealing process is possible. It can become a viable option for the manufacturing process of semiconductor devices based on ZnO films. Here, we study the synthesis of four ZnO samples, each from different zinc sources. Synthesis directly of ZnO film is independent of the compound used as the zinc source. All ZnO samples present a morphology of nanorods.

2. Experimental

For this research, we used chemical bath deposition technique to synthesis of ZnO films. For this, we used aqueous reaction solutions with four different zinc salts

*e-mail: temistocles.mendivil@unison.mx

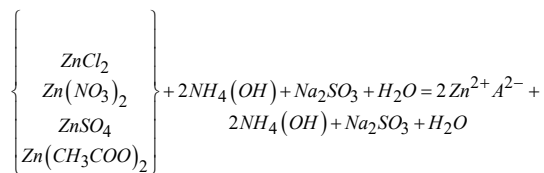
at 70 °C for 2 hours with no stirring. The used substrates are corning microscope slides made from soda lime glass. Those do not require of exhausting clean process, just are clean by using the deionized water and drying. We prepare the chemical reaction by mixing the stock reagent volumes specified in Table 1. According to a prescribed sequence, prepare the chemical reaction at the final volume of 50 ml. After we have immersed the substrate in the reaction for 5 minutes, briefly extract it from the solution and then reinsert it. Wait until you reach the two-hour deposit time.

The initial composition of the resulting reaction solutions was 0.120 M zinc salt, 0.060 M ammonium hydroxide (NH_4OH), and 0.010 M sodium sulfite (Na_2SO_3). The four zinc salts were: (1) zinc chloride (ZnCl_2), (2) zinc nitrate ($\text{Zn}(\text{NO}_3)_2$), (3) zinc sulfate (ZnSO_4), and (4) zinc acetate ($\text{Zn}(\text{CH}_3\text{COO})_2$). We emphasize that the solvent used in all the reaction solutions was tri-distilled water. Consider that following all these specifications allows the direct synthesis of ZnO. Without requiring an annealing process, as shown in the Results and Discussion section.

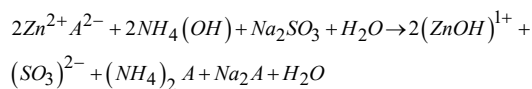
After the synthesis of the films, a D2 Phaser Bruker was used for the X-ray diffraction (XRD) analysis from 20 to 70°. Diffuse reflectance measurement used a Cary 5000 UV-Vis-NIR spectrophotometer with superb photometric performance in the 175–3300 nm. An InVia™ confocal Raman microscope was used from 50 to 1200 cm^{-1} ; the exciting wavelengths used were 488 and 785 nm. The micrographs of the deposited samples were obtained using an JSM-7800F Schottky field emission scanning electron microscope (FE-SEM). All the characterizations were at room temperature.

2.1. Generic reaction mechanism

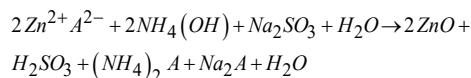
The next paragraph contains a proposal for intermediate chemical compounds to achieve Zinc Oxide from our reagents. All precursor reagents are in aqueous solutions, as the following form:



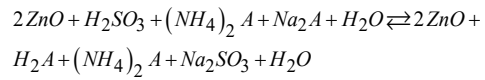
where $\text{A}^{2-} = \left\{ 2\text{Cl}^{1-}, 2(\text{NO}_3)^{1-}, (\text{SO}_4)^{2-} \text{ and } 2(\text{CH}_3\text{COO})^{1-} \right\}$ are four assayed anions.



Assumption a deprotonation process we get



Also, two of those reagents can reversibly convert into sodium sulfite plus an acid with the corresponding used anion.



3. Results and Discussion

Figure 1 presents the characterization of X-ray diffraction. It shows the diffractograms of the synthesized samples from $2\theta=20^\circ$ to 70° . By Matching experimental patterns, part a), with a database of powder diffraction patterns (PDF), part b). Crystallographic directions shown: (100), (002), (101), (102), (110), (103), (200), (112), and (201). It corresponds to a structure according to the PDF #36–1451 pattern of zincite ZnO ²⁶. In ascending order regarding preferred orientation, are accommodate the diffraction patterns. The first one is acetate, which corresponds to the zinc acetate synthesized sample. Followed by the samples listed sulfate, chloride, and nitrate, which are associated with the zinc salt corresponding. The crystalline plane (002) at 34.4° is the most intense in all the studied samples; this implies a preference for orientation along the *c* axis perpendicular to the substrate surface in all the deposited ZnO samples. The (103) plane at 62.7° is the second most intense peak for samples labeled with acetate, chloride, and nitrate. The exception was for the sulfate sample, which showed a peak (101) at 36.27° as its second most intense peak. When matching patterns of the

Table 1. Chemical recipe for synthesis of ZnO films at 70°C. It shows the order of mixing of reagents.

	Stock reagent solution or diluent	Volume (ml)
1	0.50 M zinc salt (ZnCl_2 , $\text{Zn}(\text{NO}_3)_2$, ZnSO_4 or $\text{Zn}(\text{CH}_3\text{COO})_2$)	12
2	1.00 M NH_4OH	3
3	0.10 M Na_2SO_4	5
4	Tri-distilled water	30

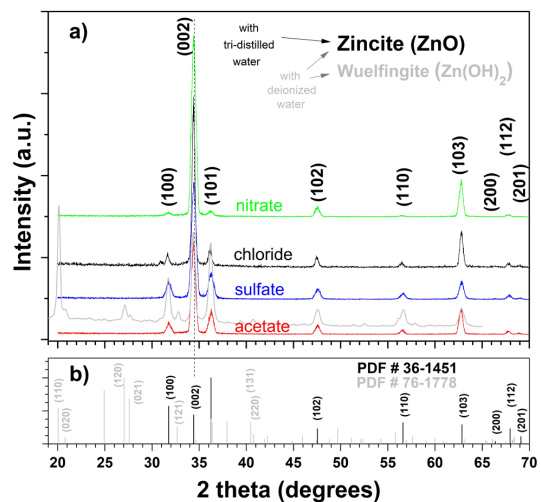


Figure 1. XRD patterns of ZnO synthesized by different salts. By Matching experimental patterns, part a), with a database of powder diffraction patterns (PDF), part b).

main peak (002) of the samples with a database, they do not present a shift of two theta lower values (strain). The effect of strain on the pattern for ZnSO₄ is not present. While for zinc chloride, all the secondary peaks present a slight shift to the left (strain). Also, there are some displacements in other peaks. We consider that the anion (SO₄)²⁻ it is better displaced than the other anions considered in our generic reaction mechanism. Then there could be more crystal density, leading to higher intensities.

We prepare samples using the identical process, resulting in affecting the growth orientation of the films via the precursor Zinc Salt. Crystals that are cross-linked grow and show X-ray diffraction patterns. Certain directions have favoring for the intensities of these patterns. This occurs both for direct and recombined X-ray diffraction. Preferred orientation or texture denotes the anisotropic dispersion of grain orientations within a material. Thin films with diverse texture properties impact the properties of applications will cause differential properties²⁷⁻³⁴.

It is important to note that neither XRD peaks corresponding to Zn(OH)₂ nor ZnS. So, an annealing process to transform this usually presented secondary phase is not required. Thus, the as-deposited material corresponds to the ZnO, independently of the used zinc salt. It with a well-defined crystalline nature associated with the hexagonal structure.

The diffraction pattern in light gray color, however, corresponds to a synthesized composite material of both ZnO and ZnOH₂. Using deionized water was the only modification made in the synthesis process, in contrast to the other approaches.

In addition, we calculate the average value of the crystallite size from the (002) plane peak with the Scherrer equation³³⁻³⁵. Crystallite sizes, resulting between 16 and 26 nm, show the nanocrystalline nature of the deposited ZnO material, see Table 2. It matches the full width at half maximum trend shown in Figure 1.

We processed the diffuse reflectance spectra of the four ZnO samples with the Kubelka-Munk equation³⁶. The results are presented in Figure 2. Here, the deposited material is transparent to wavelengths higher than about 400 nm. The material is completely opaque at wavelengths below 370 nm, in the ultraviolet region.

In the inset of Figure 2, is the energy band gap (E_g) using the Tauc approximation method³⁷. This made by plotting the square of the product of the Kubelka-Munk function (instead of optical density) and photon energy against $(E \cdot F(R))^2$ versus E .

According to this method, the calculated E_g values were 3.24, 3.22, 3.25, and 3.27 eV for the zinc salts of Zn(NO₃)₂,

Table 2. Mean crystallite size calculated from the Scherrer equation, according to the zinc salt used in the chemical formulation.

Used Zinc Salt	Mean crystallite size (nm)
ZnCl ₂	26.1
Zn(CH ₃ COO) ₂	18.8
Zn(NO ₃) ₂	18.1
ZnSO ₄	16.0

ZnSO₄, Zn(CH₃COO)₂, and ZnCl₂, respectively. These results, ranging from 3.22 to 3.27, agree with the general value of 3.3 eV reported in the literature^{1,2,5,6}.

Figure 3 presents the four Raman spectra for ZnO rods films synthesized with different zinc salts sources in the region between 50 and 1200 cm⁻¹. From top to bottom, labeled as ZnO from the different sources: ZnCl₂, Zn(CH₃COO)₂, ZnSO₄ and Zn(NO₃)₂, respectively. For comparison, the typical Raman spectra of ZnO (488 nm laser) presents phonons or vibrations corresponding to the first and second order modes³⁸⁻⁴¹. The studies attribute the normal vibrational modes at 97 cm⁻¹, 393 cm⁻¹, 410 cm⁻¹, 436 cm⁻¹, 576 cm⁻¹ to the E2(Low), A1(TO), E1(TO), E2(high), respectively. Vibrations between the broad region of 583-591 cm⁻¹ to A1(LO) and E1(LO) modes, respectively⁴²⁻⁴⁵. Therefore, the preponderant peaks are E2(high) and E2(low) which are associated with the Zn vibrational modes for the ZnO bonds⁴⁶. Among the wide region from 188 to 194 cm⁻¹, present the vibration 2E2 (Low)⁴⁶. E2(high)-E2(Low) corresponds to the vibration at 330 cm⁻¹, that involves two phonons and simultaneous absorption in E2(low) and emission in E2(high)⁴⁷.

The other intensities, around 145 cm⁻¹, 648 cm⁻¹ and 974 cm⁻¹, are commonly associated with defects or multi-phononic processes⁴². Raman peak around 660 cm⁻¹ is an intrinsic defect of ZnO⁴⁸.

In Figure 3, the gray lines denote the experimental measurements. While the color lines represent the fitting of the experimental spectra, based into FFT filter method cutoff frequency at 0.20762. Fitting provides more details for the analysis of the active modes and their variations. Also, the Raman spectra are without baselines. The spectra observed two peaks at 397 and 414 cm⁻¹, they could be A1(TO) or E1(TO) modes, respectively^{48,49}. It is worth mentioning that for define these last two Raman shift; we rely on both the experimental and theoretical part of the reference⁴⁹.

In addition, there are weak signals in the ranges 90-104 cm⁻¹ and 434-449 cm⁻¹ corresponding to vibrational modes, as well as the signals at 608 cm⁻¹ and 636 cm⁻¹. These modes correspond to the first-order phonon modes, assigned to the E2(low), E2(high), A1(low) and E1(low), respectively^{38,48-50}. The outcome confirms there are no

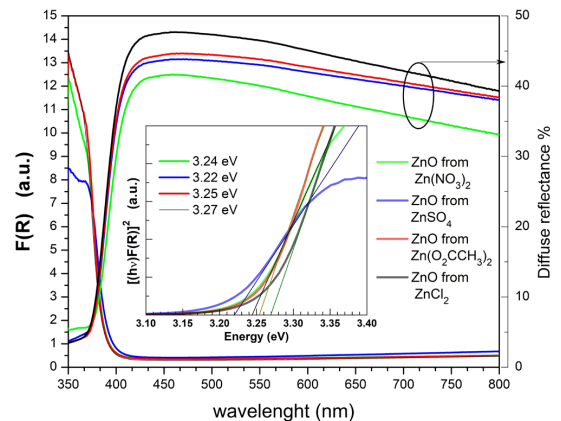


Figure 2. Diffuse reflectance, Kubelka-Munk function, and band gap of ZnO synthesized by different salts.

Table 3. Raman Shifts of the vibration modes in literature, compared with the Raman spectra of the ZnO films deposited.

vibration mode	Raman shift position (cm ⁻¹)					
	This work	Damen et al. ⁴²	Callender et al. ⁴³	Bairamov et al. ⁴⁴	Ashkenov et al. ³⁹	Chandekar et al. ^{45,46}
E_2 (L)	97	~ 101	–	~ 98	~ 102	99–97
$2E_2$ (L)	188-194	–	–	–	–	203–197
E_2 (H)- E_2 (L)	330	–	–	–	–	331–323
A_1 (TO)	384	~ 380	~ 381	~ 378	~ 380	~ 375
E_1 (TO)	411	~ 407	~ 407	~ 409.5	~ 409	~ 410
E_2 (H)	436	~ 437	~ 441	~ 437.5	~ 438	~ 437
A_1 (LO)	576	~ 574	–	~ 576	–	574–567
E_1 (LO)	582-590	~ 583	~ 583	~ 588	~ 587	~ 584

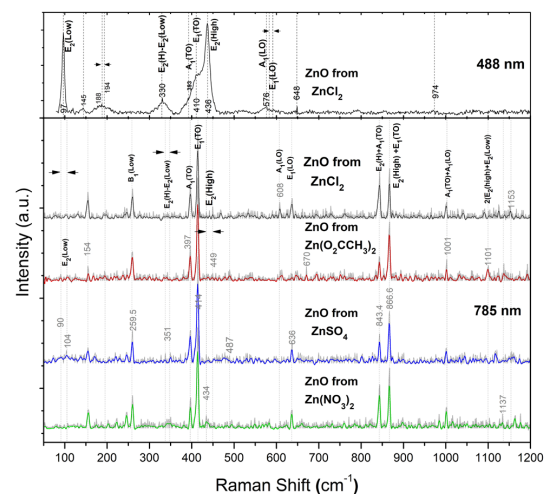
significant changes in the location of the modes. Therefore, the change in the light wavelength makes it easier to visualize the multi-phonon modes and the second harmonics. Similarly, these samples contain weak signals peaks at 154 cm⁻¹, 487 cm⁻¹, 670, 730 cm⁻¹ and 1137 cm⁻¹ among others, which some of them could be associated with noise level or another effects. Finally, the vibrational modes observed between region 337-351 cm⁻¹ and 1101 cm⁻¹ correspond to E_2 (high)- E_2 (Low) and $2(E_2$ (High) + E_2 (Low)), respectively^{38,48-50}. Regarding vibration modes in the region, 843.8 cm⁻¹ and 866.6 cm⁻¹ should be multi-phonon process or presence of defects. At about 259.5 cm⁻¹ is associated with silent mode B1⁵¹.

In Table 3, there are some of the vibrational modes for ZnO commonly used in the literature, which are also presented in this Raman analysis.

Figure 4 shows FE-SEM micrographs of four ZnO films at different magnifications with an accelerating voltage of 5 kV. The films contain nanorods of hexagonal shapes. It appreciated that the size of the nanorods is homogenous, with diameters of around 500 nm (except for Zn(NO₃)₂, which is around 250 nm). An interesting case is the ZnO synthesized from ZnCl₂, where the terminal section of the rods seems to be tubular.

As an interpretation, we want to note that the nucleation (seed formation) is different for the different Zinc precursor salts. This will imply a different orientation of the growth directions of the rods. For example, when using zinc chloride, the morphology of the rods shows a growth that is more perpendicular to the substrate. From the SEM images, the inclinations relative to the preferential growth of the crystals (002), (100), (101), (102) and (103) are validating. We relate the comparison of intensities of various peaks in the samples to the deformation effects on the crystalline lattice.

Then, singular characteristics are present to describe the surface morphology achieved for each of the zinc salts used. With zinc acetate, is detecting a growth of hexagonal rods from the center to the outside. Also, defining a well-defined stacking shape along the C axis, see Figure 4a) x40000. With zinc nitrate as a precursor,

**Figure 3.** Plot of Raman spectra of ZnO nanorods films. Experimental (gray lines) and fit model, FFT Filter method (solid black lines) with a cutoff Frequency of 0.20762.

we observe a growth of stacking hexagonal blocks with a defined diameter in the rod's formation, see Figure 4b) x40000. Using zinc sulfate as a precursor, we can note the formation of a very well-defined hexagonal rod with very smooth and homogeneous faces, see Figure 4c) x40000. Finally, when use zinc chloride, growth is stack, hollow hexagonal blocks, which are progressively filled. It grows perimeter from the outside in. They show a cavity at the growth end, which is filled, see Figure 4d), x40000, we mean the samples are not completely hollow.

Figure 5a and Figure 5b depict a selected region of the ZnO film synthesized from ZnCl₂. Here, it is possible to appreciate a single hexagonal rod arranged crosswise regarding the top view. These images are with magnifications x14000, Figure 5a), and x40000, Figure 5b), presenting two characteristic lengths. Also, can be seen in the figure that the prism reaches length slightly above 2 μm.

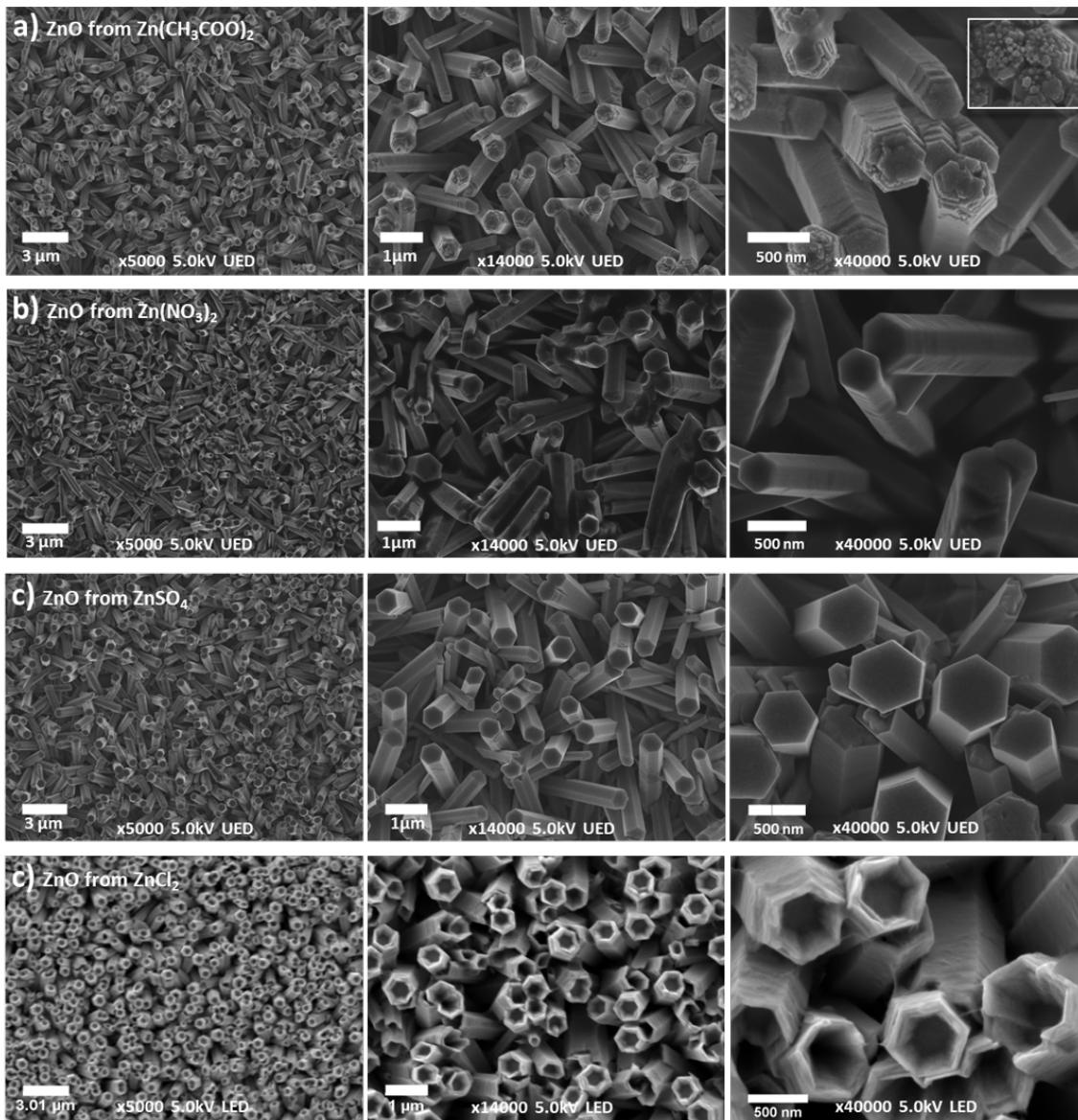


Figure 4. SEM images of ZnO films.

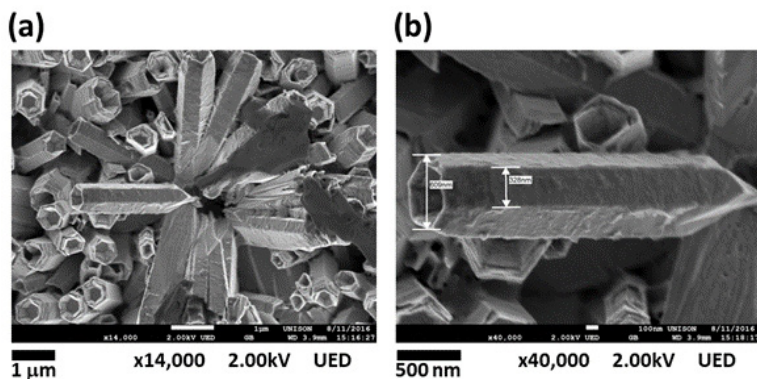


Figure 5. SEM images of ZnO from $ZnCl_2$.

4. Conclusions

Chemical bath deposition is a practical method for the direct synthesis of ZnO films. These have a well-defined hexagonal crystalline structure and high orientation. We would like to remark that sodium sulfite and tri-distilled water are imperative to get the ZnO formation. It is essential to note that sodium sulfite and tri-distilled water are crucial in the formation of ZnO in One-step synthesis. Brief removal of the substrate from the reaction after 5 min promotes the growth of the material. The ZnO material synthesized following the chemical formulation reported here presents a band gap of 3.28 eV and grows with the shape of hexagonal rods. The SEM images give us an idea of distinctive differences in the growths of the hexagonal rods depending on the precursor salt used. All these results are reproducible regardless of the zinc salt used as the zinc source. ZnO nanorods films can be deposited with no further thermal annealing, using this formulation.

5. Acknowledgments

The author M. Cortez-Valadez appreciates the support by “Investigadores por México” CONAHCYT.

6. References

- Look DC. Recent advances in ZnO materials and devices. *Mater Sci Eng B*. 2001;80(1-3):383-7. [http://dx.doi.org/10.1016/S0921-5107\(00\)00604-8](http://dx.doi.org/10.1016/S0921-5107(00)00604-8).
- Shinde VR, Lokhande CD, Mane RS, Han SH. Hydrophobic and textured ZnO films deposited by chemical bath deposition: annealing effect. *Appl Surf Sci*. 2005;245(1-4):407-13. <http://dx.doi.org/10.1016/j.apsusc.2004.10.036>.
- Mirzaeifard Z, Shariatnia Z, Jourshabani M, Rezaei Darvishi SM. ZnO photocatalyst revisited: effective photocatalytic degradation of emerging contaminants using S-Doped ZnO Nanoparticles under visible light radiation. *Ind. amp. Ind Eng Chem Res*. 2020;59(36):15894-911. <http://dx.doi.org/10.1021/acs.iecr.0c03192>.
- Borysiewicz MA. ZnO as a functional material: a review. *Crystals*. 2019;9(10):1-29. <http://dx.doi.org/10.3390/cryst9100505>.
- Srikant V, Clarke DR. On the optical band gap of zinc oxide. *J Appl Phys*. 1998;83(10):5447-51. <http://dx.doi.org/10.1063/1.367375>.
- Shinde VR, Gujar TP, Noda T, Fujita D, Vinu A, Grandcolas M, et al. Growth of shape-and size-selective zinc oxide nanorods by a microwave-assisted chemical bath deposition method: effect on photocatalysis properties. *Chemistry*. 2010;16(34):10569-75. <http://dx.doi.org/10.1002/chem.200903370>.
- Yamabi S, Imai H. Growth conditions for wurtzite zinc oxide films in aqueous solutions. *J Mater Chem*. 2002;12(12):3773-8. <http://dx.doi.org/10.1039/b205384e>.
- Sharma DK, Shukla S, Sharma KK, Kumar V. A review on ZnO: fundamental properties and applications. *Mater Today Proc*. 2022;49:3028-35. <http://dx.doi.org/10.1016/j.matpr.2020.10.238>.
- Mishra YK, Adellung R, Röhl C, Shukla D, Spors F, Tiwari V. Virostatic potential of micro-nano filopodia-like ZnO structures against herpes simplex virus-1. *Antiviral Res*. 2011;92(2):305-12. <http://dx.doi.org/10.1016/j.antiviral.2011.08.017>.
- Duggal N, Jaishankar D, Yadavalli T, Hadigal S, Mishra YK, Adellung R, et al. Zinc oxide tetrapods inhibit herpes simplex virus infection of cultured corneas [Internet]. *Mol Vis*. 2017 [cited 2023 Sep 20];23:26-38. Available from: <http://www.molvis.org/molvis/v23/26>
- Bouttier-Figueroa DC, Sotelo-Lerma M. Fabrication, and characterization of an eco-friendly antibacterial nanocomposite of galactomannan/ZnO by in situ chemical coprecipitation method. *Compos Interfaces*. 2019;26(2):83-95. <http://dx.doi.org/10.1080/09276440.2018.1472457>.
- Bouttier-Figueroa DC, García-Valenzuela JA, Cabrera-German D, Cota-Leal M, Quevedo-López MA, Rosas-Durazo A, et al. Characterization of the antibacterial galactomannan/Zn(OH)₂-ZnO composite material prepared *in situ* from a green process using mesquite seeds as a biopolymer source. *Bull Mater Sci*. 2019;42(3):1-10. <http://dx.doi.org/10.1007/s12034-019-1810-8>.
- Bouttier-Figueroa DC, García-Valenzuela JA, Cota-Leal M, Robles-Zepeda RE, Sotelo-Lerma M. Preparation, and characterization of antibacterial gels of galactomannan/Zn nanocomposite in Carbopol-based matrix using mesquite seeds as the biopolymer source. *Polym. from Renew. Resour*. 2023;14(1):3-15. <http://dx.doi.org/10.1177/20412479221135379>.
- Vyas S. A short review on properties and applications of zinc oxide based thin films and devices: ZnO as a promising material for applications in electronics, optoelectronics, biomedical and sensors. *Johns. Matthey Technol. Rev*. 2020;64(2):202-18. <http://dx.doi.org/10.1595/205651320X15694993568524>.
- Fraga MA, Furlan H, Pessoa RS, Massi M. Wide bandgap semiconductor thin films for piezoelectric and piezoresistive MEMS sensors applied at high temperatures: an overview. *Microsyst Technol*. 2014;20(1):9-21. <http://dx.doi.org/10.1007/s00542-013-2029-z>.
- Nakano M, Makino T, Tsukazaki A, Ueno K, Ohtomo A, Fukumura T, et al. Transparent polymer Schottky contact for a high performance visible-blind ultraviolet photodiode based on ZnO. *Appl Phys Lett*. 2008;93(12):123309. <http://dx.doi.org/10.1063/1.2989125>.
- Wibowo A, Marsudi MA, Amal MI, Ananda MB, Stephanie R, Ardy H, et al. ZnO nanostructured materials for emerging solar cell applications. *RSC Advances*. 2020;10(70):42838-59. <http://dx.doi.org/10.1039/D0RA07689A>.
- Muchuwani E, Sathiaraj TS, Nyakoty H. Synthesis and characterization of zinc oxide thin films for optoelectronic applications. *Heliyon*. 2017;3(4):1-18. <http://dx.doi.org/10.1016/j.heliyon.2017.e00285>.
- Ortel M, Balster T, Wagner V. Chemical composition and temperature dependent performance of ZnO thin film transistors deposited by pulsed and continuous spray pyrolysis. *J Appl Phys*. 2013;114(23):2345021. <http://dx.doi.org/10.1063/1.4846736>.
- Morita T, Ueno S, Tokunaga T, Hosono E, Oaki Y, Imai H, et al. Fabrication of transparent ZnO thick film with unusual orientation by the chemical bath deposition. *Cryst Growth Des*. 2015;15(7):3150-6. <http://dx.doi.org/10.1021/cg501729w>.
- Souletie P, Bethke S, Wessels BW, Pan H. Growth, and characterization of heteroepitaxial ZnO thin films by organometallic chemical vapor deposition. *J Cryst Growth*. 1989;86(1-4):248-51. [http://dx.doi.org/10.1016/0022-0248\(90\)90724-Y](http://dx.doi.org/10.1016/0022-0248(90)90724-Y).
- Medina-Montes MI, Baldenegro-Perez LA, Sanchez-Zeferino R, Rojas-Blanco L, Becerril-Silva M, Quevedo-Lopez MA, et al. Effect of depth of traps in ZnO polycrystalline thin films on ZnO-TFTs performance. *Solid-State Electron*. 2016;123:119-23. <http://dx.doi.org/10.1016/j.sse.2016.05.005>.
- Hodes G. Chemical solution deposition of semiconductor films. New York: Marcel Dekker; 2002. p. 39, p. 289.
- Cota-Leal M, García-Valenzuela JA. Chemical solution deposition of Al(OH)₃-AlOOH films: application for surface sensitizing of rigid and flexible substrates to improve the adhesion in coating technology areas. *ChemistrySelect*. 2021;6(24):6083-96. <http://dx.doi.org/10.1002/slct.202101449>.
- Muslih EY, Munir B. Emerging solar energy materials. United Kingdom: IntechOpen; 2018. p. 49.
- JCPDS: Joint Committee on Powder Diffraction Standards. Powder diffraction file #36-1451. Newtown Square: The International Centre for Diffraction Data; 2023.

27. Zyoud SH, Ahmed NM, Lahewil ASZ, Omar AF. Micro spot ZnO nanotubes using laser assisted chemical bath deposition: A low-cost approach to UV photodetector fabrication. *Sens Actuators A Phys.* 2022;338:113485. <http://dx.doi.org/10.1016/j.sna.2022.113485>.
28. Elzawiei YS, Abdulhameed A, Hashim MR, Halim MM. A study of the UV photodetectors properties based on the effect of TiO₂ on ZnO nanorods grown via the chemical bath deposition method on p-type Si (100) substrates. *Opt Mater.* 2023;144:114353. <http://dx.doi.org/10.1016/j.optmat.2023.114353>.
29. Al-Khazali SMS, Al-Salman HS, Hmood A. Low cost flexible ultraviolet photodetector based on ZnO nanorods prepared using chemical bath deposition. *Mater Lett.* 2020;277:128177. <http://dx.doi.org/10.1016/j.matlet.2020.128177>.
30. Sultana J, Paul S, Saha R, Sikdar S, Karmakar A, Chattopadhyay S. Optical and electronic properties of chemical bath deposited p-CuO and n-ZnO nanowires on silicon substrates: p-CuO/n-ZnO nanowires solar cells with high open-circuit voltage and short-circuit current. *Thin Solid Films.* 2020;699:137861. <http://dx.doi.org/10.1016/j.tsf.2020.137861>.
31. Chen J, Li C, Song JL, Sun XW, Lei W, Deng WQ. Bilayer ZnO nanostructure fabricated by chemical bath and its application in quantum dot sensitized solar cell. *Appl Surf Sci.* 2009;255(17):7508-11. <http://dx.doi.org/10.1016/j.apsusc.2009.03.091>.
32. Gu P, Zhu X, Yang D. Vertically aligned ZnO nanorods arrays grown by chemical bath deposition for ultraviolet photodetectors with high response performance. *J Alloys Compd.* 2020;815:152346. <http://dx.doi.org/10.1016/j.jallcom.2019.152346>.
33. Scherrer P. Bestimmung der Größe und der inneren Struktur von Kolloidteilchen mittels Röntgenstrahlen. *Nachrichten von der Königlichen Gesellschaft der Wissenschaften zu Göttingen. Mathematisch-Physikalisch Klasse.* 1918;1918:98-100.
34. Warren BE. X-Ray diffraction. Mineola: Dover Publications, Inc.; 1990. 253 p. Republication of the work originally published by Addison-Wesley Pub. Co., 1969.
35. Saravanan R, Prema Rani M. Metal and Alloy bonding: an experimental analysis: charge density in metals and alloys. London: Springer-Verlag; 2012. p. 26. <http://dx.doi.org/10.1007/978-1-4471-2204-3>.
36. Murphy AB. Modified Kubelka-Munk model for calculation of the reflectance of coatings with optically-rough surfaces. *J Phys D Appl Phys.* 2006;39(16):3571-81. <http://dx.doi.org/10.1088/0022-3727/39/16/008>.
37. Tauc J. Optical properties and electronic structure of amorphous Ge and Si. *Mater Res Bull.* 1968;3(1):37-46. [http://dx.doi.org/10.1016/0025-5408\(68\)90023-8](http://dx.doi.org/10.1016/0025-5408(68)90023-8).
38. Cuscó R, Alarcón-Lladó E, Ibáñez J, Artús L, Jiménez J, Wang B, et al. Temperature dependence of Raman scattering in ZnO. *Phys Rev B Condens Matter Mater Phys.* 2001;75(16):165202. <http://dx.doi.org/10.1103/PhysRevB.75.165202>.
39. Ashkenov N, Mbenkum BN, Bundesmann C, Riede V, Lorenz M, Spemann D, et al. Infrared dielectric functions and phonon modes of high-quality ZnO films. *J Appl Phys.* 2003;93(1):126-33. <http://dx.doi.org/10.1063/1.1526935>.
40. Yahia SB, Znaidi L, Kanaev A, Petit JP. Raman study of oriented ZnO thin films deposited by sol-gel method. *Spectrochim Acta A Mol Biomol Spectrosc.* 2008;71(4):1234-8. <http://dx.doi.org/10.1016/j.saa.2008.03.032>.
41. Zhou H, Chen L, Malik V, Knies VC, Hofmann DM, Bhatti KP, et al. Raman studies of ZnO:Co thin films. *Phys Status Solidi, A Appl Mater Sci.* 2007;204(1):112-7. <http://dx.doi.org/10.1002/pssa.200673019>.
42. Damen TC, Porto SPS, Tell B. Raman effect in Zinc oxide. *Phys Rev.* 1966;142(2):570-4. <http://dx.doi.org/10.1103/PhysRev.142.570>.
43. Callender RH, Sussman SS, Selders M, Chang RK. Dispersion of Raman cross section in CdS and ZnO over a wide energy range. *Phys Rev, B, Solid State.* 1973;7(8):37883-3798. <http://dx.doi.org/10.1103/PhysRevB.7.3788>.
44. Bairamov RH, Heinrich A, Irmer G, Toporov VV, Ziegler E. Raman study of the phonon halfwidths and the phonon: plasmon coupling in ZnO. *Phys Status Solidi, B Basic Res.* 1983;119(1):227-34. <http://dx.doi.org/10.1002/psb.2221190126>.
45. Chandekar KV, Shkir M, Al-Shehri BM, AlFaify S, Halor RG, Khan A, et al. Visible light sensitive Cu doped ZnO: facile synthesis, characterization, and high photocatalytic response. *Mater Charact.* 2020;165:1-11. <http://dx.doi.org/10.1016/j.matchar.2020.110387>.
46. Chandekar KV, Shkir M, AlFaify S, Al-Shehri BM, Al-Namshah KS, Hamdy MS. A noticeable consistent improvement in photocatalytic efficiency of hazardous textile dye through facile flash combustion synthesized Li-doped ZnO nanoparticles. *J Mater Sci Mater Electron.* 2021;32(3):3437-50. <http://dx.doi.org/10.1007/s10854-020-05090-z>.
47. Guo S, Du S, Dai S. Analysis of Raman modes in Mn-doped ZnO nanocrystals. *Phys Status Solidi, B Basic Res.* 2009;246(10):2329-32. <http://dx.doi.org/10.1002/psb.200945192>.
48. Abdelouhab ZA, Djouadi D, Chelouche A, Touam T. Structural, morphological and Raman scattering studies of pure and Ce-doped ZnO nanostructures elaborated by hydrothermal route using nonorganic precursor. *J Sol-Gel Sci Technol.* 2020;95(1):136-45. <http://dx.doi.org/10.1007/s10971-020-05293-0>.
49. Thyri J, Österlund L, Edvinsson T. Polarized and non-polarized Raman spectroscopy of ZnO crystals: method for determination of crystal growth and crystal plane orientation for nanomaterials. *J Raman Spectrosc.* 2021;52(8):1395-405. <http://dx.doi.org/10.1002/jrs.6148>.
50. Taziwa R, Ntozakhe L, Meyer E. Structural, morphological and Raman scattering studies of carbon doped ZnO nano-particles fabricated by PSP technique. *J Nanosci Nanotechnol Res.* 2017;1:1-3.
51. Musa I, Qamhieh N, Mahmoud ST. Synthesis, and length dependent photoluminescence property of zinc oxide nanorods. *Results Phys.* 2017;7:3552-6. <http://dx.doi.org/10.1016/j.rinp.2017.09.035>.